Indian Journal of Engineering & Materials Sciences
Vol. 29, December 2022, pp. 730-737
DOI: 10.56042/ijems.v29i6.70315

Experimental Investigation on Dimensional Characteristics and Surface Morphology of Microchannels Fabricated on Smart Ceramic by DPSS Nd:YAG Laser

Samir Kumar Panda[a], Sweta Rout[b], Debasish Panigrahi[b], & Debabrata Dhupal[a*]

[a]Department of Production Engineering, Veer Surendra Sai University of Technology, Burla 768 018, India

[b]Department of Mechanical Engineering, National Institute of Technology, Rourkela 769 008, India

Received: 9 September 2022; Accepted: 17 October 2022

Smart ceramic material like barium titanate ($BaTiO_3$) is in high demand in today's highly competitive precision industries; as it has numerous applications in electronic, biomedical, and aerospace engineering.In this endeavor, laser micro-milling approach (LMMA) hasbeenattempted with a suitable experimental design plan; to scrutinize the laser influencing variables against the LMMA outcomes during the processing of $BaTiO_3$ throughout the fabrication of microchannels. This article presents an investigational act on the fabricated micro-channels to discern the impacts of LMMA parameters (gas pressure, scan strategy, current and scanning speed) against the dimensional (like deviations in channel upper and lower width) and surface characteristics of the surface feature. The surface morphology study hasbeen accomplished with the support of energy dispersive spectroscopy (EDS) in conjunction with scanning electron microscope (SEM) to scrutinize the elemental alterations and surface characteristics at the zone of laser ablation. A statistical multi-objective optimization (MOO) technique known as grey relational analysis (GRA) has beenused later in this paper to predict an optimal parametric setting. The MOO results' efficacy has been validated further in the corroboration assessments, the predicted optimal solutions have been obtained with an error of 4.57 %, 3.89 % and 4.88 % for W-RCL, LWD and UWD respectively.

Keywords: Laser Micro-Milling Approach (LMMA), Microchannels, $BaTiO_3$, Smart-ceramic, Multi-objective optimization (MOO)

1 Introduction

Modern manufacturing industries address the challenges, which have beenencountered during processing of advanced engineering materials, where non-traditional machining plays an important role. Machining of advanced engineering materials (mainly smart ceramic materials) by traditional methods is complex due to various issues like breakage of a tool, generation of thrust force which causes high power, and lack of surface rectitude[1]. However, these advanced engineering materials (i.e. like smart ceramics) are widely accepted in different industrial applications. Processing ofthese materials is not that easy; thus, one of the dynamic processes in manufacturing has needed to fabricate exact components with minimal dimensional change. Non-traditional machines are highly efficient in dealing with these materials because of their high productiveness. For this reason, they seek more attention from all the researchers[2–6].

Smart ceramics are the sensitive ceramic materials, which have the ability to acclimate to alteration when expose to outer environment. These materials are classified into three kinds: pyroelectric, ferroelectric and piezoelectric. When stressed, these piezoelectric ceramics generate an external electric field on their surface, and later these electric fields generate stress. Barium titanate ($BaTiO_3$) is one of the piezoelectric ceramicswidely used in various micro-devices including Microelectromechanical Systems (MEMS). MEMS applications include energy harvesting, transducers for medical purpose, and actuators in automotive and aerospace components[7].

The processing of smart ceramic materials (mainly $BaTiO_3$) requires certain careful consideration to raise the quality standard. Laser-based subtractive machining process has evolved to produce various micro and macro aspects in a broad range of materials.

It has several advantages, including the ability to machine exact complex shapes, the absence of tooling costs, and other issues that make it cost-effective[8,9].

Current research has demonstrated the viability of using laser to create micro features on a variety of advanced engineering materials, including AISI 304 SS[10], aluminum nitride[11], Calcium phosphate-Alumina[12], DD6 nickel superalloy[13], Inconel-718[14], Poly-methylmethacrylate[15], nitinol[16], Silicon[17], basalt–glass hybrid composite[18], titanium[19], zirconia toughened

*Corresponding author (E-mail: debabratadhupal@gmail.com)

alumina[20], aluminum oxide[21], Silicon nitride[22], Duplex stainless steel[23], Bio-lox forte[24], and Zirconia[25].

According to current research, the laser based subtractive process, i.e., laser micro-milling approach (LMMA), has been employed to generate micro-channels on different advanced ceramic materials. Mohammed *et al.*[26] have used Nd: YAG direct laser writing to study the effect of parametric variables like the intensity of the laser, scan strategy, and pulse overlap while fabricating micro-channels on alumina ceramic. They have found the impact of these process variables on the responses like channel's depth, material ablation rate, top, and bottom width error. Fabrication of micro-channels on zirconia by Nd: YAG laser has been stated by Abdo *et al.*[25]; where in the influence of the parameters like scanning speed, pulse intensity, and pulse frequency on the channel's dimensional accuracy, and surface quality has been scrutinized. The results have shown that surface roughness can be controlled by the scanning speed and laser intensity, which has the most significant influence for the top width error. A pulsed Nd: YAG laser has been adopted to generate micro-grooves on silicon nitride by Dixit *et al.*[22]. The authors have studied the influence of process variables like scanning speed, lamp current, and pulse frequency on groove dimensions, and defects on surfaces (like surface roughness, heat-affected zone).

The authors[27] have adopted a nanosecond laser to perform micro-channels by using a micro-milling approach. They have considered the influential parameters such as layer thickness per scan, scanning speed, pulse frequency, and laser intensity as controlling factors. Further, they have analyzed their impact on dimensional channel characteristics (depth, upper & lower width, and taper angle on the right and left side of micro-channel). Zhu *et al.*[28] have adopted a picosecond laser for fabricating microgrooves on hydroxyapatite. Further they have analyzed the laser parameters like focal plane position, scanning velocity, scanning times, high voltage level, and pulse frequency and their significant impact on microgrooves depth and width. They have also reported the effect of parameters on the alteration in the elemental composition of ablated and non-ablated zones and the thermal damages. Generation of micro-channels on bio-lox-forte with the assistance of nanosecond laser is stated[24].Further, they have evaluated the critical input parameters in the ranges like laser intensity (86 – 96) %, pulse frequency (5–25) kHz, track displacement (5– 20) μm, scanning speed (100 – 500) mm/s, and scanning strategies (cross, net, and line) and have analyzed their impact on the channel's geometrical accuracy, MRR, surface roughness, and surface morphology during machining. Rout *et al.*[5] have defined that the pulsed laser in nanosecond wavelength range as a promising substitute to avert the poor machining performance during laser machining of yttria-partially stabilized zirconia by adopting a novel technique. The authors have generated micro-channels by adopting the laser micro-milling approach. They have considered the process variables like pulse frequency, current, pulse width, and scanning speed and have analyzed their impact on the dimensional accuracy, HAZ, and microstructural analysis. Dixit *et al.*[21] have fabricated U-shaped microgrooves on alumina using Nd: YAG laser and have studied the input parameters like frequency, scanning speed, pulse width, current, and gas pressure on the dimensional accuracy of the groove.

However, most of the previous studies have fixated on the open-air micro-drilling, micro-grooving, and micro-channeling of structural and bio-ceramics. According to the existing literature, scarcely any survey has been reprinted in the past literature related to nanosecond laser micro-milling of smart ceramic material ($BaTiO_3$) under gas-assisted conditions, particularly for dental applications. This piezoelectric material generates an electric charge due to mechanical stress, and when implanted inside the mouth, it heals infected gums by generating electricity. As a result, the current research has demonstrated its novelty by going through those discussions and can be applied in the medical field, such as dentistry.

The current research has been focused on using argon gas to fabricate micro-channels over $BaTiO_3$. In the study, we have attempted LMMA by utilizing a novel parameter like strategy for laser scan type (SS), i.e., 0°mode and 45°angular mode with parametric comparison over a smart ceramic material. The current endeavor has been focused on the experimental investigation of distinct scanning arrangements (i.e., laser beams in angular or straight-line position) and other operating factors like scan speed, gas pressure and current for this LMMA. The surface and geometrical characteristics of micro-channels have been scrutinized in the later part of this article by interconnecting themwith the most essential operating factors.

Moreover, a mathematical multi-purpose optimization method namely, GRA has been utilized for the prediction of best settings of parameters. However, for an adequate analysis in the context of parametric influences, a study of variable-response interaction effects has done from the graphs along with a surface

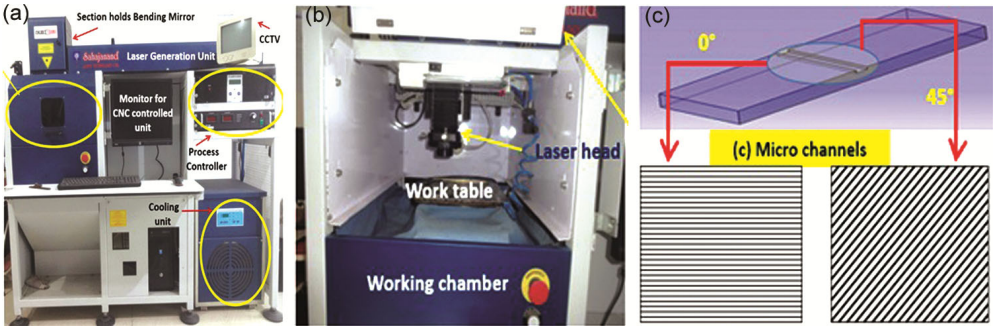

Fig. 1 — Image of Pulsed Nd: YAG laser machine setup and micro-channels under 45° and 0°

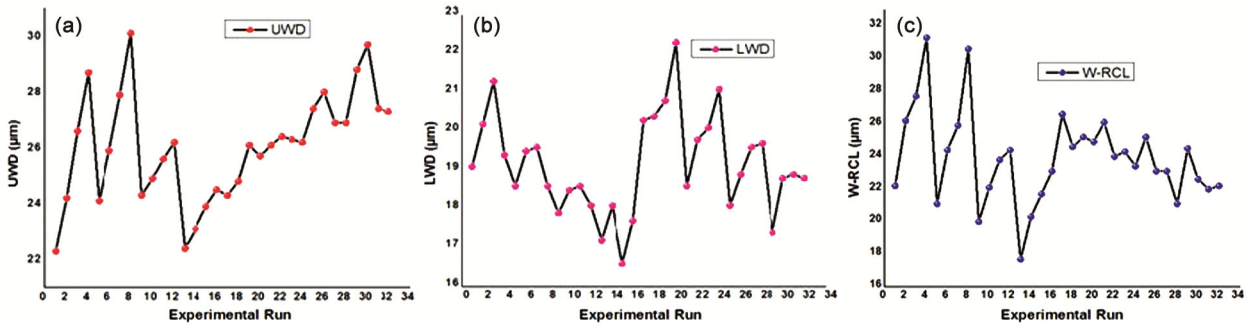

Fig. 2 — Experimental no. vs. responses (a) UWD, (b) LWD, and (c) W-RCL.

analysis study using SEM and EDS. This analysis has been performed to inspect the manufactured surface of $BaTiO_3$; which reflects the novel contribution for the present work.

2 Materials and Methods

The work-piece material in this experimental investigation is a Barium titanate ($BaTiO_3$) sheet of dimension 25mm x 25mm x 3mm. The chemical composition (in weight percentage) and the mechanical, electrical and thermal properties of $BaTiO_3$ are enlisted in Table 1. In this study, experimentations were conducted with the support of a 75 W Nd-YAG pulsed laser with a polarized beam powered CNC system (model: SPRIGO LD) for the LMMA on the work-piece surface. An argon (Ar) gas supply unit was attached to the machining set up with the coaxial nozzle system having diameter of 1 mm. The schematic view of the Nd:YAG pulsed laser machine is represented in Fig. 1.

In this study, 32 set of experimentations were conducted as per the DOE plan followed by GRA multi-objective-optimization (MOO) to scrutinize the process parameters (gas pressure, scanning strategy, current, and scanning speed) and their impacts during the LMMA act.

The LMMA variables and their levels (available in Table 2), were considered to study the impact on the chosen responses during the LMMA, namely, recast layer's width (W-RCL), deviations in upper width (UWD) and lower width (LWD).

Table 1 — Properties of $BaTiO_3$

Property	Value
Density	6.06 g/cm3
Fusion point	1250 °C
Melting point	1625 °C
Thermal conductivity	6 W/mK
Electrical conductivity	10-2 s/cm
Resistivity	50 µΩ
Young's modulus	67 GPa

Table 2 — Input factors and their levels for LMMA

Parameters	Unit	L-1	L-2	L-3	L-4
Scan Strategy	deg. (°)	0°	45°	-	-
Diode current	A	16	18	20	22
Gas pressure	kg/cm^2	0.3	0.4	0.5	0.6
Scan Speed	mm/s	0.5	0.7	0.9	1.1

However, the remaining parameters were taken as constant throughout the experimentation (i.e., the number of passes is 6, pulse width 8% and pulse frequency 3 kHz). After four iterations over the fabricated channel surface, the values in average of each LMMA outcomes were considered for effective utilization of results to assess current objectives of research. The results are depicted in Fig. 2, which represents the response characteristics concerning each set of parametric settings.

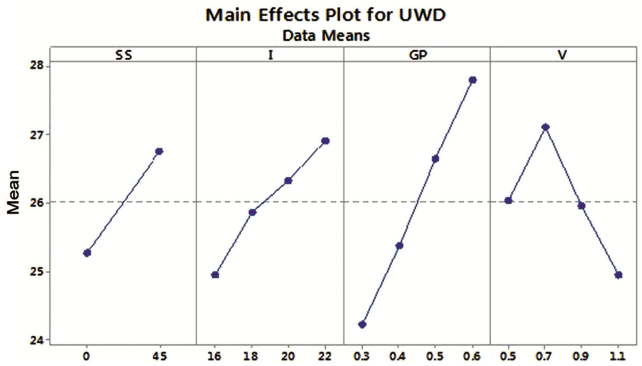

Fig. 3 — Main effects plot for UWD

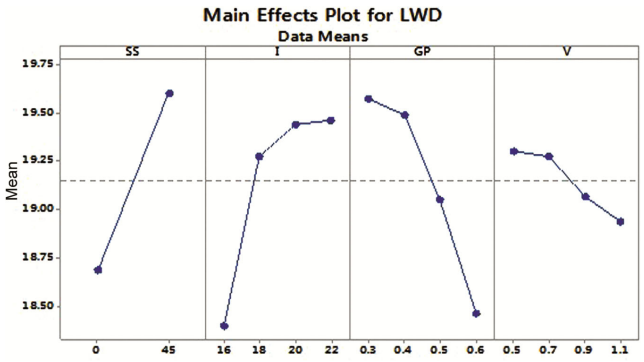

Fig. 4 — Main effects plot for LWD

3 Results and Discussion

In this research, the LMMA was adopted to produce micro-channels on $BaTiO_3$ by adopting the desired DOE plan.

The interaction of process parameters relative to the chosen responses (i.e. UWD, LWD and W-RCL) are illustrated in Fig. 3, Fig. 4, and Fig. 5 to describe the impacts of LMMA variables on the response characteristics of micro-channels in this current endeavor. However, the dimensional peculiarities and the surface morphology study of the fabricated micro-channels were investigated through EDS and SEM reports.

3.1 Parametric study on the micro-channel dimensions

Considering the influencing variables like GP, I, SS, and v into account, micro-channels were created on the target substrate. From the main effects plots of Fig. 3 and Fig. 4, the parametric impacts on the micro-channels' dimensional characteristics (i.e., LWD and UWD) were investigated. The parametric investigation revealed that I and GP variables as a single factor, have a significant impact on the micro-channels' width. It has been evident from the Fig. 3 and Fig. 4 that, with the rising in I and GP values, UWD and LWD values increase noticeably; while, the values of UWD and LWD decline with increase in v levels.

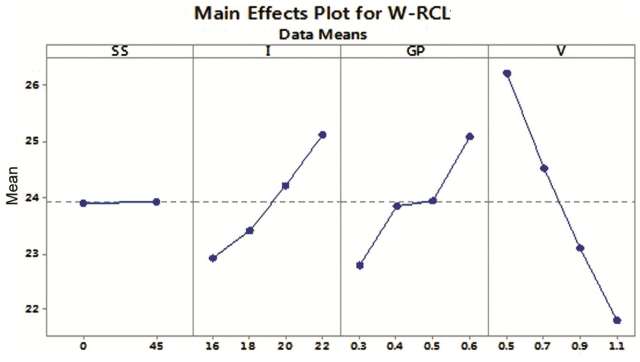

Fig. 5 — Main effects plot for W-RCL

The reason behind for these trends of graph is the effect of laser intensity. As, I levels increase, it tends to enhance the intensity of laser up to such high levels that the temperature gets elevated at the interaction zone of laser and target material. Hence the laser cutting process continues with a down values of v[5,21]. But the higher GP values corresponding to this case effectively expel the molten-material by minimizing the material's reflectivity from the laser interaction zone of target substrate.

Moreover, at SS of 45°, the scan was initially at 0°, and subsequently the movement was at an inclination of 45° over the $BaTiO_3$ surface. In this SS, the ablation process occurred due to the double modes of scan. This results in a larger width at the domain of laser scan during the laser-material interaction; which consequences in large deviations in channel geometrical characteristics.

However, at the reduced values of GP, the inert gas was ineffectively utilized; this leads to distribute the gas molecules insignificantly over the $BaTiO_3$ surface at elevated levels of I. Furthermore, at the declined v levels, the interaction of laser at the $BaTiO_3$ surface was more for the extended period; resulting in a substantial deviation in micro-channel's dimension. Some SEM views of channels are illustrated in Fig. 6, which describes the smaller, moderate and wider sections of the micro-channels' width in different experimental runs during LMMA of $BaTiO_3$.

3.2. Parametric study on micro-channel surface

Figure 5 shows the LMMA variables and their impacts on the W-RCL values. The uneven distribution of recast along the micro-channel boundaries was observed during the generation of micro-channels. The molten materials those erupted from the laser-$BaTiO_3$ interaction were further rapidly condensed and re-solidified, forming a layer known as the recast deposition layer. The recast layer formation appears due

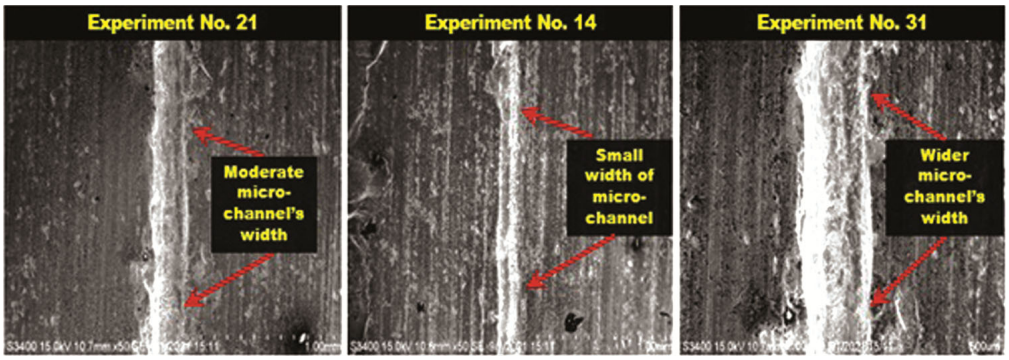

Fig. 6 — SEM images of micro-channels' width processed on $BaTiO_3$

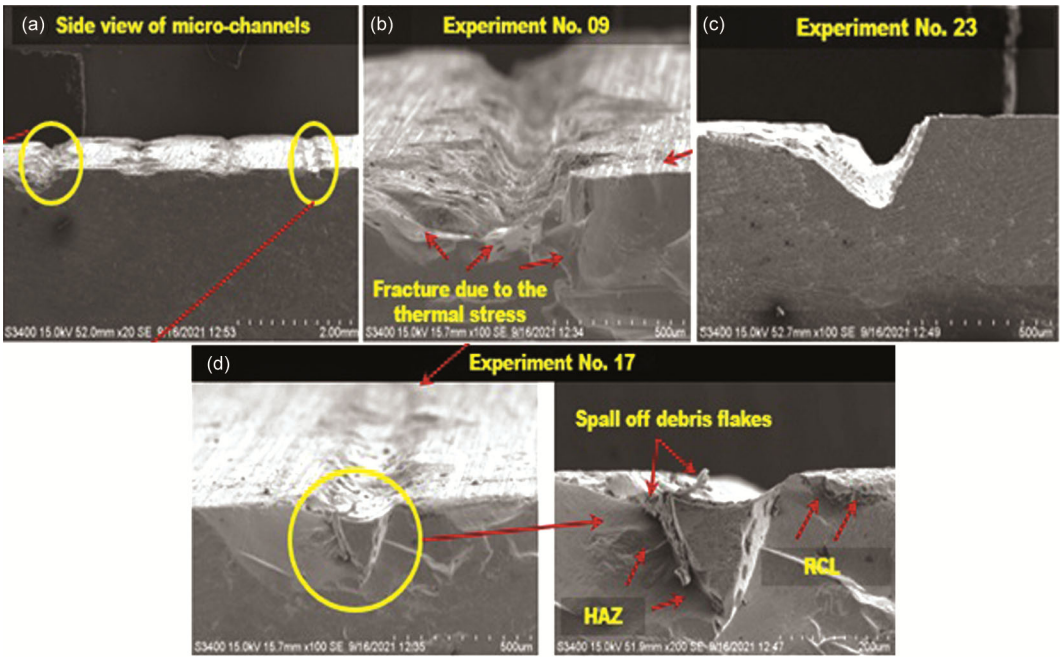

Fig. 7 — SEM images of LMMA processed $BaTiO_3$ surface.

to the spallation[29]; the SEM images of micro-channels surfaces are illustrated in Fig. 6 and Fig. 7.

The pulse current and the scanning speed levels are the most influential factor in the generation of RCL. As the I levels rise, the ablated zone's mean temperature increases, and the materials (i.e. at the liquefied condition) spatters away from zone of the melting; this further forms a thick RCL along the side walls of micro-channels. However, with the raise in I levels, the intensity of pulsed laser was more.

These consequences in wider W-RCL at the elevated thermal energy and at the reduced levels of v. Moreover, at the higher GP levels, the value of recast width increases significantly due to the assist gas's cooling effect. Higher levels of I, leads to form more molten materials at the laser-interaction spot on the material's surface. However, at this stage raise in the levels of GP, affect the micro-channel surface adversely with its cooling action; which, consequences in the formation of a dense recast layer and significant material distortion[12].

However, 45° mode of scan provided lower values of W-RCL when compared to the 0° scan mode. The laser beam moved twice at the 45° scanning strategy, initially at 0° and then at 45°. The formation of RCL in LMMA can be understood with the support of such statement that, as the recast material re-melted sporadically during the multiple scan of the laser beam. As a result of the induced recoil pressure during the vaporization of molten material that was previously in a liquid state, it was suppressed by the GP values. This mechanism is dependent on the processing material's absorbed energy at the machining area; supports to accumulate the melted material in a liquefied state.

Due to these reasons, W-RCL is inversely proportional to the time period for re-melting of material which bids in a liquid form per unit scale. The laser movement was twice at SS of 45°; as a result, the laser beam scan path overlapped and the melted material exploded outside. These liquefied material further set beside the micro-channels regardless of multiple scans of laser; as a result, the W-RCL was slightly more at SS of 45° compared to 0° scan[30,31].

3.3 MOO with GRA

Grey Relational Analysis (GRA) is a statistical tool of grey system, which is extensively used to optimize the desired responses by using GRG (i.e. grey relational grade). Several researchers[32–35] have incorporated to optimize the values of controllable parameters for significant achievement while using the multi-objective criterion via GRG. The normalization of responses was accomplished by using the criterion (i.e. lower is better type) according to the responses that to minimize the fabricated surface and dimensional errors. The steps mentioned in Eq.(1)-Eq.(4) were utilized for supporting the multi-criterion optimization by GRA [12,36,37].

Step-1: Normalization of responses by following the Eq. (1)

$$\vartheta_j(q) = \frac{\mathrm{MAX}\phi_j(q) - \phi_j(q)}{\mathrm{MAX}\phi_j(q) - \mathrm{MIN}\phi_j(q)} \quad ...(1)$$

Step-2: Calculation for Deviational sequences by using the Eq. (2)

$$\Delta_{0j}(q) = \left|\vartheta_0(q) - \vartheta_j(q)\right| \quad ...(2)$$

Step-3: GRC were determined using Eq. (3)

$$\boldsymbol{\lambda}_j(q) = \frac{\Delta_{\min} + \phi\Delta_{\max}}{\Delta_{0j}(q) + \phi\Delta_{\max}} \quad ...(3)$$

Step-4: Evaluation of the GRG values were accomplished by using the Eq.(4)

$$\Psi_j = \frac{1}{n}\sum_{j=1}^{n}\lambda_j(q) \quad ...(4)$$

Where, $\vartheta_0(q)$: reference sequences; ϕ: identification coefficient (ranges between 0 to 1); n: 32; Ψ_j : GRG values determined for the j^{th}experiment;$\vartheta_j(q)$: j^{th} experimental run in comparability sequences after pre-processing, $\Delta_{0j}(q)$: deviation sequences; $\boldsymbol{\lambda}_j(q)$: GRC of individual responses as a function of minimum ($\Delta_{\min}$) and maximum ($\Delta_{\max}$) deviations of each response variable and $\phi_j(q)$: the initial sequence for the mean of responses. The optimal parametric setting of 1.1 mm/s, 0.3 kg/cm^2 ,16 A and 0ᵎ was obtained with the 1st rank for the overall objectives towards minimizing the values of W-RCL, LWD and UWD.

3.4 Surface morphology study

A selected region is magnified and revealing the grain morphology in the melting zone which changes dramatically compared to the microstructure of base material. From Fig. 8 one could find that microstructures in the HAZ, base material and the recast zone are distinctly different. Figure. 8 carry a magnified SEM view of channel bed surrounded with oxide globules, ejected detritus and micro-cracks. This formation of cracks and pores are mainly observed at the base and recast layer along with the sidewalls of the micro channels; this results because of the higher value of diode current and assists gas pressure. At this condition, the material melts rapidly, and due to the increased in the flow of gas, the material cool faster, which leads to contracting suddenly and generates cracks.

The laser parameters are also played a vital role in the formation of different imperfections like spall off debris flakes, fracture during LMMA. The splash patterns represent the ejection of material from the channels in the form of ejected detritus and oxide globules; when these droplets of ejected materials deposited in and along the channel surface, this results in recast layer. During laser machining, surface distortions are the most important physical characteristics that cause the formation of packets of re-solidified material in all the fabricated micro-channels and channel-wall. Moreover, it is shown that the recast layer thickness of the channels is thinner, mainly resulting from the expelling/flowing effects.

Before machining, the primary chemical elements of barium titanate (BaTiO3), such as barium (Ba), titanium (Ti), oxygen (O), carbon (C), cerium (Ce), and vanadium (V), can be identified from Fig. 9.

However, after machining, there is an alteration in the elemental ratios of the base material; from the compositions, some were increased and some were decreased. However, four EDS readings were taken in each representative zone (before machining zone, channel bed, and recast layer), as shown in Fig. 9.

After machining, the level of oxygen and carbon ratios increases compared to the base material. Later on, the metal oxide is formed in the resolidified zone, expanding the O level by declining the base element

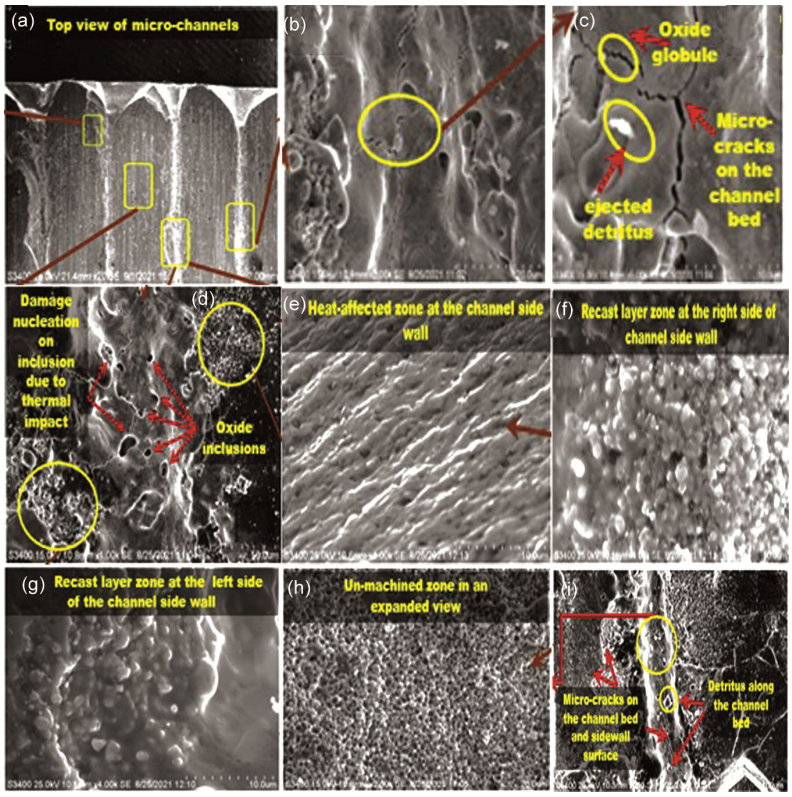

Fig. 8 — SEM image of micro-channelsin different aspects

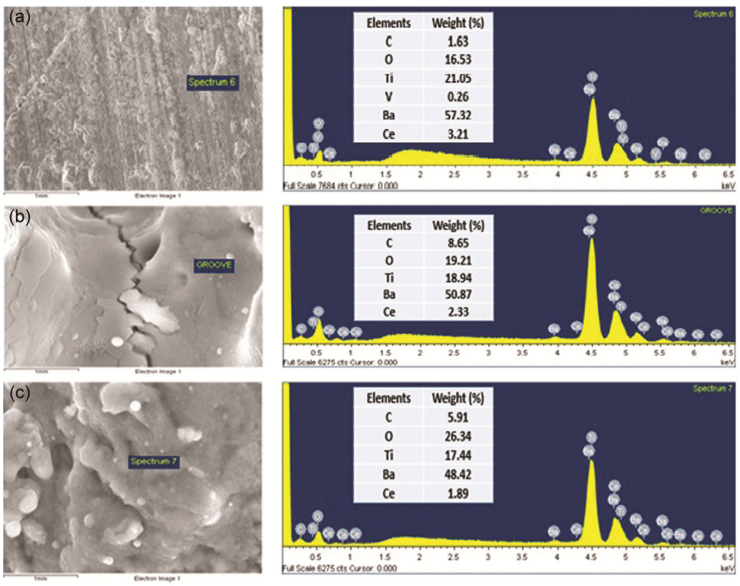

Fig. 9 — EDS report of (a) before machining zone, (b) channel bed, and (c) recast layer

of the metal. The lattice spacing of oxides is greater than that of the component of base metals.

3.5 Confirmation test

The efficacy of the GRA predicted optimal results were validated further in this research. Three reiterations of experiments were carried out with the support of predicted optimal parametric settings in order to assess the uncertainty of physical experimentation. The measurements were repeated three times with SEM, and the average values were used to assess the GRA-MOO's effectiveness.

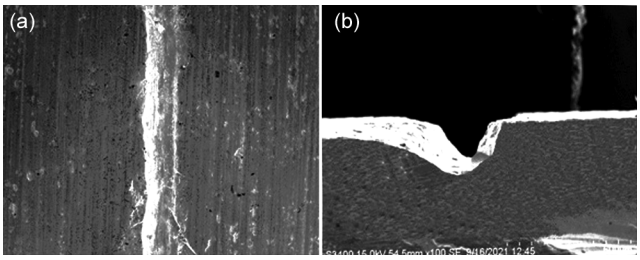

Fig. 10 — SEM view of channel under optimal parametric setting.

The preeminent SEM images of micro-channels from those three experiments are depicted in Fig. 10, and the best results were obtained as errors of 4.57%, 3.89%, and 4.88% for W-RCL, LWD, and UWD, respectively, based on the assessments made during corroboration.

4 Conclusion

The following attainable outcomes that have been noted throughout this current research are listed in this section.

- Out of all the input variables, GP and I are most important variables in fabricating micro-channels on the $BaTiO_3$.
- It has observed that from two scanning strategies, an angular scanning mode of 45° is a perfect scanning mode to achieve; a good channel surface with a low recast layer compared to 0°.
- GRA has been used to optimize the LMMA parameters. The optimal parametric setting of v: 1.1 mm/s, GP: 0.3 kg/cm^2, I: 16 A and SS: 0° has been obtained with the 1st rank for the overall objectives towards minimizing the W-RCL, LWD and UWD values i.e, 17.7µm, 17.2 µm and 22.4 µm respectively and errors of 4.57 %, 3.89 % and 4.88 % have obtained for W-RCL, LWD and UWD from the confirmation test.
- (iv) Further more, the surface morphology study has revealed that increased GP and SS values combined with a low current level can produce a significant surface feature.

References

1 Staehle RW, *Mater Sci Eng A* 198 (1995) 245.
2 Pradhan S, Das RS, Jena PC & Dhupal D, *Adv Mater Process Technol 83 (2021) 1714*.
3 Panigrahi D, Rout S, Patel KS & Dhupal D, *Int J Adv Manuf Technol,* 112 (2021) 133.
4 Farooq UM, Ali MS, He Y, Khan AM, Pruncu CL, Kashif M, Ahemad N & Asif N, *J Mater Res Technol,* 9 (2021) 16186.
5 Rout S, Panigrahi D, Patel KS & DhupalD, *Opt Lasers Eng,* 144 (2021) 106654.
6 Pradhan S, Tripathy SS & Dhupal D, *Adv Mater Process Technol* 82 (2021) 596.
7 Mems T, Eom C, & Trolier-mckinstry S, Thin-film piezoelectric MEMS, (2021) 1007.
8 Raj D, Reddy RVB, Maity RS & Pandey MK, *Mater Today Proc*, 18 (2019) 98.
9 Meijer J, *J Mater Proc Tech* 149 (2004) 2.
10 Jadhav A & Kumar S, *Adv Mater Process Technol* 5 (2019) 429.
11 Wang L, Zhao W, Mei X, Yang Z, Shen X & Liu H, *Ceram Int* 46 (2020) 24018.
12 S, Dhupal D & Kumar B, *Mater Today Proc* 5 (2018) 24133.
13 Zhang Z, Wang W, Jiang R, Zhang X, Xiong Y, & Mao Z, *Opt Laser Technol,* 121 (2020)105834.
14 Shrivastava PK, Singh B, Shrivastava Y, Pandey AK & Nandan D, *Proc Inst Mech Eng Part C, J Mech Eng Sci* (2019) 1.
15 Khoshaim AB, Elsheikh AH, Moustafa EB, Basha M, & Showaib EA, J Mater Res Technol (2021) 235.
16 Pradhan S, Dash PB, & Kumari K, *Adv Mater Process Technol,* (2021) 1.
17 Allahyari E, Nivas JJJ, Valadan M, & Granata V, *Opt Laser Technol* 126 (2020) 106073.
18 Jain A, Singh B, & Shrivastava Y, *Inst Mech Eng Part C J Mech Eng Sci* (2019) 1.
19 Muthuramalingam T, Moiduddin K, Akash R, Krishnan S, Mian SH, Ameen W, & Alkalefah H, *Opt Laser Technol* 132 (2020) 106494.
20 Saini KS & Dubey KA, *J Manuf Process*, 44 (2019) 349.
21 Ranjan S, Sudhansu D, Das R & Dhupal D, *J Ind Eng Int*, 15 (2019) 333.
22 Dixit SR, Panigrahi D, Rout S, Panda S,& Dhupal D,Lasers Eng, 49 (2021) 319.
23 Panigrahi D, Rout S, Sanket S, Patel SK & Dhupal D, Mater Today Proc 44 (2021) 1916.
24 Abdo BMA, Anwar S, El-tamimi AM, Alahmari AM, & Nasr EA, *Precis Eng* 53 (2018) 179.
25 Abdo BMA, El-tamimi AM, Anwar S, Umer U, Alahmari AM, & Ghaleb MA, *Int J Adv Manuf* 98 (2018) 2213.
26 Khan M, Umer U, & Al-ahmari A, *J Manuf Process 41 (2019) 148.*
27 Abdo AMB, Ahmed N, El-tamimi MA, Anwar S, Alkhalefah H, & Nasr AE, 33 (2019) 1.
28 Zhu H, Zhang Z, Xu J, Xu K & Ren Y, *Precis Eng* 54 (2018) 154.
29 Liu Y, Liu L, Deng J, Meng R, Zou X, & Wu F, *Ceram Int* 8 (2017) 6519.
30 Feng S, Zhang R, Huang C, Wang J, Jia Z & Wang J, *Mater Sci Semicond Process* 105 (2020) 104701.
31 Wang XY, Ng GKL, Liu Z, Li L, & Bradley L, *Thin Solid Films* 454 (2004) 84.
32 Li Z, Zhang F, Luo X, Chang W, Cai Y & Zhong W, *J Eur Ceram Soc* 39(2019) 705.
33 Girish BM, Siddesh HS, & Satish BM, *SN Appl Sci* 1 (2019) 937.
34 Song H, Dan J, Li J, Du J, Xiao J & Xu J, *J Manuf Process* 38 (2019) 9.
35 Pu Y, Zhao Y, Meng J, Zhao G. & Liu Q, *Materials*14 (2021) 529.
36 Kumar S, Mitra B & Kumar N, *Grey Sys Theo App* 9 (2019) 449.
37 Sylajakumari P A, Ramakrishnasamy R & Palaniappan G, *Materials* 11 (2018) 1743.